Charge transition levels of nitrogen dangling bonds at Si/SiO_2 interfaces: A first-principles study

Philipp Dahinden, Peter Broqvist, and Alfredo Pasquarello
Institute of Theoretical Physics, Ecole Polytechnique Fédérale de Lausanne (EPFL), CH-1015 Lausanne, Switzerland and Institut Romand de Recherche Numérique en Physique des Matériaux (IRRMA), CH-1015 Lausanne, Switzerland
(Received 26 August 2009; revised manuscript received 25 January 2010; published 26 February 2010)

The defect levels of the nitrogen dangling bond at the Si/SiO_2 interface are determined through a density-functional approach. The composition grading at the interface is modeled through crystalline and amorphous models of stoichiometric SiO_2, nitrided SiO_2, and substoichiometric silicon oxides. The relevant charge transition levels are first determined with respect to the band edges of the parent oxides within a semilocal density-functional scheme. Through the use of band edge shifts and band offsets previously obtained with hybrid functionals, the calculated defect levels are then positioned with respect to a band diagram of the Si/SiO_2 interface which shows good agreement with the experimental one. We find that the $0/-$ charge transition level locates within the Si band gap. The level locates close to the Si valence band for nitrogen atoms in the stoichiometric oxide, but is found to rise across the silicon band gap as the environment of the nitrogen atoms becomes more silicon rich. The latter raise is accompanied by a stabilization of the incorporated nitrogen.

DOI: 10.1103/PhysRevB.81.085331 PACS number(s): 73.20.−r, 71.55.−i

I. INTRODUCTION

Reliability issues in semiconductor electronics are often directly related to point defects occurring at the atomic level,[1] which generally localize at interfaces where the structural mismatch occurs. Such interface effects become increasingly important when the size of the device shrinks.[2] In order to improve the reliability of these devices, it is therefore crucial to acquire a detailed knowledge of the defects that are present. Both experimental and theoretical methods have been deployed to identify and study these defects. Experimentally, point defects can be studied with electron paramagnetic resonance (EPR) measurements.[3,4] However, this technique works only for paramagnetic defects and does not provide information about the position of the energy level with respect to the band edges. Capacitance-voltage $(C-V)$ measurements on the other hand give information about the position of the defect level inside the band gap, but do not allow the identification of its atomic structure. On the theoretical side, first-principles calculations allow the atomic modeling of the defect structures as well as the determination of the defect energy levels, but the latter are only useful insofar meaningful comparisons with experiments can be carried out.

An example of a well studied interface is the Si/SiO_2 interface.[4,5] Silicon dioxide is extensively used as a dielectric in metal-oxide-semiconductor (MOS) devices because it can be grown relatively easily by thermal oxidation on a Si substrate and the resulting interface shows a sufficiently small amount of interface states. However, as the thickness of the gate dielectric decreases, phenomena such as leakage currents or dopant diffusion occur.[6] Nitrided silicon oxides have been found to effectively deal with these problems.[7] Furthermore, nitrogen also improves the dielectric properties of the oxide layer. However, the incorporation of nitrogen at the interface is known to increase the densities of interface traps,[8] causing performance degradations and reliability problems.[9–11] In particular, N has been seen to amplify the negative bias temperature instability (NBTI), a critical reliability issue in integrated circuits that continues to be a problem in devices with high-κ gate dielectrics.[12,13] For further improvement of the devices, it is therefore important to identify which kind of defects are introduced by the addition of nitrogen. EPR measurements in silicon oxynitrides yield rather complex spectra containing several peaks, not all of which have been unanimously identified.[14–17] One possible defect is the nitrogen dangling bond (or nitrogen bridging N_b center), that occurs through depassivation of the N-H bond of the $(Si)_2$-N-H configuration. Upon illumination, nitrogen dangling bonds have clearly been observed by EPR measurements in nitrided silicon dioxide films on silicon.[18] The $(Si)_2$-N-H configuration has also been invoked to explain x-ray photoemission spectra of silicon oxynitrides grown by plasma-enhanced chemical vapor deposition.[19] However, experimental characterization of the energy levels of this defect center is still lacking. As an illustration, Fig. 1 shows a plot of the spin-polarization of the nitrogen dangling bond defect in silicon oxide. The singly occupied orbital has p character

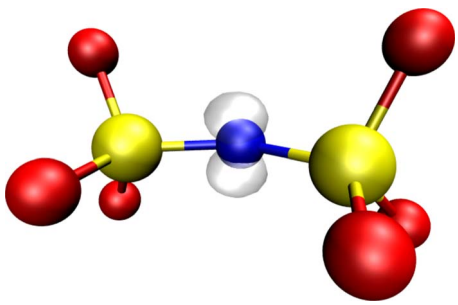

FIG. 1. (Color online) Isosurface of the spin polarization for the neutral nitrogen dangling bond defect in silicon oxide. The central N atom (blue, dark gray) is shown with its nearest-neighbor Si atoms (yellow, light gray) and its second-nearest-neighbor oxygen atoms (red, medium gray). The spin polarization (transparent) has the characteristics of a p-orbital perpendicular to the plane defined by the Si-N-Si chain.

and is oriented perpendicular to the plane defined by the Si-N-Si chain.

First-principles methods using density-functional theory have been successful in electronic structure calculations and are increasingly being used to gain understanding of defects at the atomic scale.[20] However, theoretical modeling of defect energy levels is not straightforward. First of all, most common methods based on semilocal functionals, such as the generalized gradient approximation (GGA), severely underestimate band gaps of semiconductors and insulators. As a result, direct comparison between theory and experiment is not possible. By including a certain fraction of exact nonlocal exchange energy, hybrid functionals have recently been shown to yield band offsets at semiconductor-oxide interfaces in agreement with experiment.[21,22] However, a generalized application of this method to interface defects is still computationally prohibitive. The same consideration also applies to alternative methods such as the many-body perturbation theory in the GW approximation.[23] A second difficulty in the study of defects results from the modeling of the interface. The treatment of structural disorder and of charged defects at interfaces still represents a nontrivial task for simulation.

In this paper, we investigate charge transition levels of nitrogen dangling bonds at the Si/SiO_2 interface within a density-functional approach. The structure in the transition region is modeled through a series of bulk structures which account for the disordered nature of the oxide and for its composition grading. First, the charge transition levels are determined with respect to the oxide band edges within a semilocal density-functional scheme. Then, band edge shifts and band offsets calculated through the use of hybrid functionals[22] are used to obtain a description that matches the experimental band diagram of the Si/SiO_2 interface. In this way, the calculated defect levels can be located with respect to the band edges of silicon. Furthermore, we study the dependence of the defect level on the oxidation state of the nearest neighbor Si atoms as the Si concentration increases in the substoichiometric oxide.

This paper is organized as follows. The adopted methodology is described in Sec. II. In particular, the treatment of a physical interface by means of bulk calculations as well as the interpretation scheme based on hybrid functionals are discussed. The different oxide models are described and analyzed in Sec. III. The nitrogen dangling bond defect levels are presented in Sec. IV. Finally, Sec. V collects the conclusions that can be drawn from this work.

II. METHODOLOGY

A. Computational scheme

All the models used in this work have undergone full structural relaxation within a semilocal density-functional scheme. The electronic structure was described through the generalized gradient approximation introduced by Perdew, Burke, and Ernzerhof (PBE).[24] This approximation was preferred over the local density approximation because of consistency with previous hybrid functional results[21,22] which are used in the analysis. We used the spin-polarized functional for properly describing unpaired electrons. We used a scheme based on plane-wave basis sets and ultrasoft pseudopotentials.[25] The energy cutoffs were set at 31 Ry for the wave-function expansion and at 124 Ry for the charge density.[26,27] The defect level calculations were performed in supercells, with a Brillouin zone sampling limited to the Γ point unless specified otherwise. The structural relaxations were performed using a nonlinear minimization technique introduced by Broyden, Fletcher, Goldfarb, and Shanno.[28] We used the PWSCF code of the QUANTUM ESPRESSO[29] package.

B. Alignment

The determination of charge transition levels requires the calculation of total energies of charged defect states. The use of periodic boundary conditions in typical simulation setups leads to spurious electrostatic interactions due to the compensating background charge. While correction terms have been proposed for charged defects in homogeneous dielectric environments,[30] the analogous treatment in the presence of interfaces is less trivial. To circumvent this problem, we modeled the structure at the Si/SiO_2 interface, through a series of bulk silicon oxide models of varying oxygen concentration. The dielectric conditions in the models vary between those of silicon and those of SiO_2, as the oxygen concentration in the models is increased. While this description does not reproduce the specific dielectric conditions at the interface, it should nevertheless cover the range over which the dielectric polarization varies in the transition region.

This modeling scheme is viable provided the electronic structures of the various models can correctly be aligned. To define a proper alignment scheme, we investigated the behavior of the deep O $2s$ states across a superlattice model of the Si/SiO_2 interface generated previously.[31] The electronic density of states was projected on the O $2s$ orbital for every oxygen atom. For each atom, we then calculated an average O $2s$ level. In Fig. 2(a), we plot the variation in these energies as oxygen atoms across the oxide layer are considered. The figure considers oxygen atoms belonging to both the substoichiometric and stoichiometric oxide. Individual levels are quite scattered over a window of about 0.5 eV. Their average level shows a smoother dependence with a raise of the order of 0.1 eV in the substoichiometric region. In order to unveil any systematic correlation, we studied in Fig. 2(b) the dependence of the O $2s$ levels at the interface on the average of oxidation state of the two neighboring Si atoms. This figure reveals a systematic correlation by which the O $2s$ level raises by ~ 0.3 eV for the low oxidation states of Si.

Throughout this work, we adopted an alignment scheme by which the electronic structures of the considered models are aligned by setting their average O $2s$ level to that in stoichiometric SiO_2. This choice carries the advantage of a transparent alignment scheme, but neglects the raise observed for silicon-rich environments. As shown in the following, consideration of this raise only reinforces the observed trends, without altering any of the qualitative observations. Its effect on the low oxidation states is recalled when appropriate. An alignment scheme based on deep

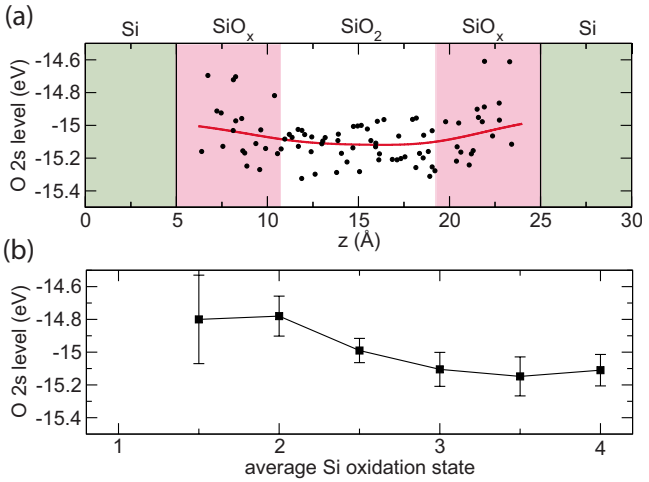

FIG. 2. (Color online) (a) Average O 2*s* level across a superlattice model of the Si/SiO_2 interface. For every O atom, the average O 2*s* level is determined from the local density of states projected on the considered atom. The (red) curve corresponds to an average in which the atomic contributions are weighted through Gaussian distributions centered on the atoms and broadened by a standard deviation of 1.5 Å. The substoichiometric transition region connecting the Si substrate to the SiO_2 oxide is indicated. In (b), the O 2*s* level is plotted vs the average oxidation state of its two neighboring Si atoms. The represented data points correspond to averages and the error bars indicate the standard deviations.

atomic levels has already successfully been used for other defects at oxide-semiconductor interfaces.[32–34]

C. Band-edge corrections

The band-gap underestimation of semilocal density-functional approaches is one of the major obstacles which prevents the situation of calculated defect levels within a band diagram that allows for comparison with experiment. To overcome this difficulty we relied on two recent results. First, it has been shown that energy levels of localized defect states determined within a semilocal density-functional approach do not undergo important shifts when calculated within a hybrid functional approach of higher accuracy, provided the two calculations are aligned through a common reference level.[21] In particular, this shift amounts to only 0.1 eV for the $0/-$ charge transition level of the nitrogen dangling bond in α-quartz SiO_2,[21,35] which is representative of the defects studied in the present work. This result implies that defect levels calculated within a semilocal density-functional scheme are already accurately determined, despite the band-gap problem. Hence, this result indicates that the correction of the defect levels and that of the band edges are issues that can be dealt with separately. The second result concerns the determination of the corrected band edges. For this it is necessary to have recourse to electronic structure approaches of higher accuracy than in semilocal density-functional schemes. The method of choice is the GW many-body perturbation scheme,[36] but it has been shown that accurate results can also be achieved through the use of hybrid functionals.[22] Indeed, the application of the latter functionals

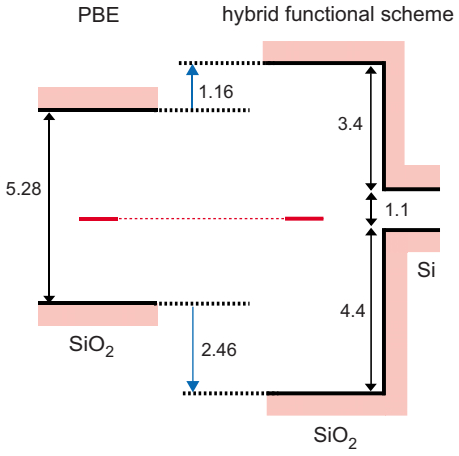

FIG. 3. (Color online) Applied scheme to position defect levels obtained through semilocal density-functional calculations within a band diagram of the Si/SiO_2 interface which virtually coincides with the experimental one. The scheme is based on the hybrid functional results obtained in Refs. 21 and 22. Energies are in eV.

to the determination of band offsets at semiconductor-oxide interfaces has resulted in very accurate band diagrams.[22] In particular, for the Si/SiO_2 interface that is of interest to the present study, the theoretical band diagram agrees with experiment within less than 0.1 eV.[22]

As a consequence, it is possible to locate charge transition levels in the experimental band gap by the following procedure.[37] First, charge transition levels and band edges are calculated with respect to the band edges of the respective oxide models within a semilocal density-functional scheme (e.g., the PBE). Second, the electronic structures of the various oxide models are aligned to that of the amorphous SiO_2 model through the O 2*s* levels. Third, the band-edge shifts derived through the use of hybrid functional calculations are applied.[21,22] This step is illustrated in Fig. 3. On the basis of the results obtained in Ref. 22, it consists in displacing the conduction band upwards by 1.16 eV and the valence band downwards by 2.46 eV. Fourth, the band edges of silicon are then determined through the valence band offset of 4.4 eV, as obtained within a hybrid functional scheme.[22] In this way, the calculated defect levels are positioned within a band diagram which virtually corresponds to the experimental one.

III. OXIDE MODELS: STRUCTURAL AND ELECTRONIC PROPERTIES

The model structures used in this work have different origins and can be classified into three groups. The first one includes models of crystalline and amorphous stoichiometric SiO_2. The second group consists of models of nitrided silicon oxide. The third group comprises substoichiometric oxide structures, including both crystalline and manually disordered structures. An overview of all models and of their principal characteristics is given in Table I. The Kohn-Sham densities of states (DOS) pertaining to the model structures are shown in Fig. 4. The positions of the valence and conduction band edges of the defect-free host structure are indicated.

TABLE I. Overview of the different models studied in this work. N_{at} is the number of atoms in the supercell used for the defect calculation and ρ is the density in g/cm^3. Bond lengths (d) are given in Å and bond angles (θ) in degrees. E_g is the band gap (in eV). E_{corr} is the correction term (in eV) appearing in Eq. (1) for a charge $q=\pm 1$. N_{bulk} specifies the number of individual bulk structures considered, and N_{subst} is the number of defect models that resulted from the bulk models. Values in parentheses correspond to standard deviations and refer to the least significant digit reported.

Model	N_{at}	ρ	$d_{Si\text{-}O}$	$d_{Si\text{-}Si}$	$\theta_{Si\text{-}O\text{-}Si}$	$\theta_{O\text{-}Si\text{-}O}$	E_g	E_{corr}	N_{bulk}	N_{subst}
Stoichiometric SiO_2										
a-SiO_2	72	2.20	1.63(2)		132(13)	109(6)	5.3	0.44	1	7
α quartz	72	2.53	1.65(1)		144(1)	110(1)	5.7	0.45	1	1
β cristobalite	96	2.22	1.629(1)		142(1)	109(1)	5.8	0.38	1	1
Nitrided SiO_2										
SiO_xN_y	101	2.20	1.64(2)		146(12)	109(5)		0.39	3	3
Substoichiometric SiO_2										
crystalline 3+	60	2.18	1.640(5)	2.333(4)	153(7)	109(2)	4.5	0.32	1	1
disordered 3+	60	2.23	1.64(1)	2.36(3)	148(9)	109(3)	4.1	0.32	1	5
crystalline 2+	128	2.13	1.647(4)	2.381(5)	177(3)	109(3)	0.2	0.19	1	1
disordered 2+	128	2.20	1.65(1)	2.40(4)	157(11)	109(5)	1.5	0.19	1	10
crystalline 1+	144	2.22	1.663(1)	2.384(1)	165.0(1)	109(4)	0.2	0.14	1	1

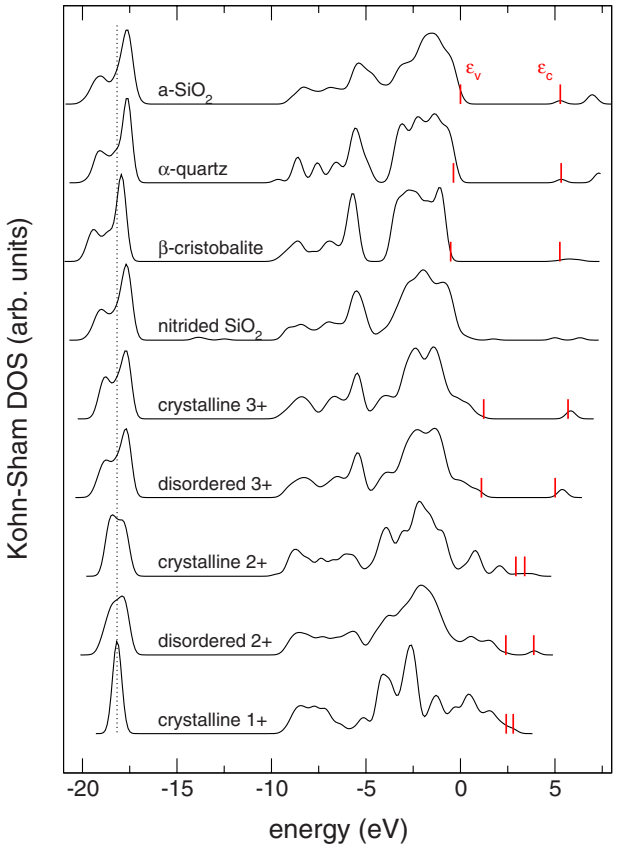

FIG. 4. (Color online) Comparison of the normalized Kohn-Sham DOS of all models. The DOSs are aligned through the average oxygen 2s level (dotted line). The energy scale is referred to the edge of the valence band of a-SiO_2. The valence (ε_v) and conduction (ε_c) band edges are indicated for all defect-free models. A Gaussian broadening with a standard deviation of 0.3 eV was used.

A. Stoichiometric SiO_2

The crystalline models of SiO_2 comprise both α quartz and β cristobalite. The model of α quartz contains 72 atoms in an orthorhombic supercell at a density of 2.53 g/cm^3, with dimensions $9.95\times 8.63\times 10.9$ Å^3. The structure shows a mean Si-O bond length of 1.65 Å and a Si-O-Si angle of 144°. For this structure, we calculated a band gap of 5.7 eV.

The model of β cristobalite was obtained starting from what is generally called "ideal" β cristobalite, i.e., a cubic Si diamond lattice with oxygen atoms placed between every pair of Si atoms. Then, the O atoms were moved out of their central positions in order to allow for the SiO_2 tetrahedra to rotate during structural relaxation.[38] The initial model contained 24 atoms. Both lattice parameters and internal cell coordinates were fully relaxed. The rotations observed during relaxation were antiparallel for neighboring SiO_2 tetrahedra, as has recently been suggested in Ref. 38 in order to arrive at the symmetry $I\bar{4}2d$. However, at variance to Ref. 38, the rotation axes in our model were not parallel to either of the main crystal axes. Nevertheless, the final structure was characterized by an energy gain of 0.05 eV per SiO_2 unit compared to the ideal structure, in agreement with the energy gain obtained in Ref. 39. Furthermore, the volume decreased by 13%, qualitatively similar to the value of 9% found in Ref. 39. The final supercell used for the defect calculations contained 96 atoms at a density of 2.22 g/cm^3, with dimensions $10.1\times 10.1\times 14.0$ Å^3. We computed a band gap of 5.8 eV.

A model of amorphous SiO_2 (a-SiO_2) had been obtained previously via *ab initio* molecular dynamics techniques[40,41] and consists of a 72-atom supercell at a density of 2.20 g/cm^3. We used a cubic supercell of side 10.3 Å. Relaxation of the atomic coordinates in the PBE gave an average Si-O bond length of 1.63 Å and a mean Si-O-Si angle

$132 \pm 13°$. This structure shows a band gap of 5.3 eV. The slight differences in the structural and electronic properties with respect to the original model[40,41] result from the present use of the PBE rather than the local density approximation. In the following, we refer to this structure as to the amorphous SiO_2 model, while it is understood that the disorder in this model is limited to a periodically repeated network of only 72 inequivalent atoms. Nevertheless, this model is expected to accurately describe the local disorder around the N defects.

B. Nitrided SiO_2

Models of nitrided SiO_2 were obtained through classical molecular dynamics simulations. We used a supercell containing 34 Si, 65 O, and 2 N atoms in order to satisfy electron counting rules. The size of the cubic simulation cell was chosen to be 11.51 Å, corresponding to a density of 2.20 g/cm^3. The empirical interaction potential included terms for two- and three-body interactions.[42] After equilibration of the system at a temperature of 6000 K, it was cooled down in an exponential quenching scheme over a period of 240 ps. It was held typically 10 ps at a given temperature before reducing the temperature to the next level. From the set of obtained models, three structures contained one threefold coordinated and one twofold coordinated N atom. In addition to the nitrogen dangling bond, all three models contained up to three other atomic defects. We encountered Si dangling bonds and nonbridging oxygen atoms. None of these defects occurred in the immediate neighborhood of the N atoms. These defects were passivated by hydrogen in order to eliminate their electric activity. Subsequently, the models were structurally relaxed within our density-functional scheme. These models show an average Si-O-Si angle of 146° (see Table I).

In order to identify the location of the electronic states of the N atoms in the nitrided silicon oxide, we show in Fig. 5 the projected DOS on the atomic orbitals of the two nitrogen atoms. The DOS of a-SiO_2 is also shown for comparison. The states with energies ranging between −15 and −10 eV correspond to N 2s states. The 2p states are found to mainly lie in the valence band of the host structure at energies of −10 eV or higher. The twofold coordinated N atom clearly shows a Kohn-Sham level in the band gap of a-SiO_2.

C. Substoichiometric oxides

The crystalline suboxide models were generated according to a scheme introduced by Hamann.[43] Each model is characterized by the oxidation state of the silicon atoms, which denotes the number of oxygen nearest neighbors. Starting from the ideal β-cristobalite structure described earlier (oxidation state 4+), we removed the oxygen atoms along certain directions in order to generate the model structures pertaining to lower oxidation states. For the model "crystalline 3+," all O atoms in the [111]-directed bonds were removed. For the model with oxidation state 2+, the atoms along [111] and $[\bar{1}\bar{1}1]$ were removed. In the model "1+," only the O atoms in the [111] direction were kept.

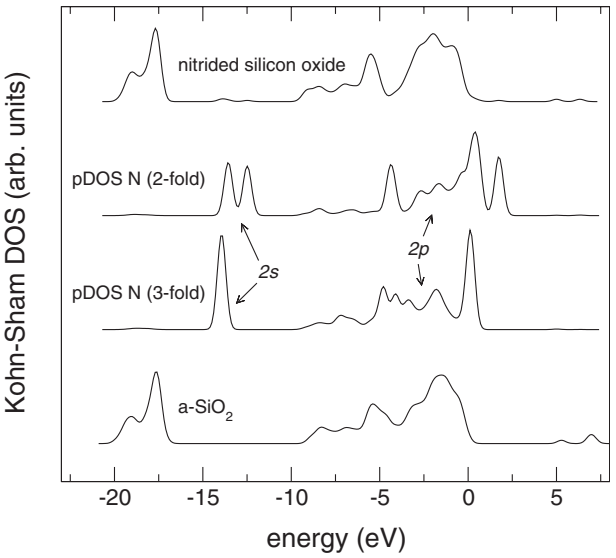

FIG. 5. Normalized Kohn-Sham DOS of a nitrided silicon oxide model and the projected DOS (pDOS) on the atomic orbitals of the twofold and threefold coordinated nitrogen atoms. The atomic character of the states is indicated. The energy scales have been aligned as in Fig. 4. For comparison, the DOS of a-SiO_2 is also shown. A Gaussian broadening with a standard deviation of 0.3 eV was used.

Optimized structures were obtained through structural relaxation of lattice parameters and of internal cell coordinates. Due to the occurrence of continuous Si-Si chains, we used a high density of k points to accurately sample the Brillouin zone.[43] In contrast to the models generated by Hamann,[43] the oxygen atoms were moved out of their central position before the structural relaxation. The reason for this is that a Si-O-Si angle smaller than 180° is expected to facilitate the defect incorporation upon N substitution at the O site. The densities obtained upon full relaxation of the crystalline models with oxidation state 3+, 2+, and 1+ are 2.18, 2.13, and 2.22 g/cm^3, respectively. For the 3+ oxidation state, we obtained a 60-atom orthorhombic supercell with dimensions $8.94 \times 10.2 \times 10.4$ $Å^3$. For the 2+ oxidation state, the 128-atom supercell is monoclinic with lattice parameters $a=c=13.4$ Å, $b=12.8$ Å, and $\beta=106°$. The 1+ model contains 144 atoms and is described by an orthorhombic supercell with dimensions $13.6 \times 15.6 \times 12.2$ $Å^3$. The band gap decreased from 4.5 eV for the oxidation state 3+ to 0.2 eV for the oxidation states 1+ and 2+. The average values for both Si-O and Si-Si bond lengths tend to increase with decreasing oxidation state (see Table I), in accord with previous investigations.[43–46]

To further corroborate the quality of our models, we compared bond energy penalties with previous results in the literature.[43–45] Penalty energies describe deviations with respect to a bond energy picture and are defined for every partial oxidation state of silicon. The bond energy reference for each oxidation state is obtained by interpolation of the total energy per Si atom in pure silicon and in the model 4+. In order to facilitate the comparison with previous work,[43,45] the 4+ model with straight bonds (i.e., ideal β cristobalite) has been chosen as reference for the interpolation. The comparison is shown in Table II. The agreement

TABLE II. Calculated bond energy penalties per Si atom ΔE (in eV) for the partial oxidation states of silicon, compared to results obtained by Hamann (Ref. 43) and by Bongiorno and Pasquarello (Ref. 45).

Oxidation state	ΔE	Ref. 43	Ref. 45
3+	0.24	0.24	0.22
2+	0.54	0.51	0.51
1+	0.52	0.47	0.50

with the values obtained in Refs. 43 and 45 is very good.

Disordered suboxide models were obtained by manual modification of their crystalline counterparts. Some of the oxygen atoms were displaced from their original location to the center of a nearby Si-Si bond. Therefore, the average oxidation state of the Si atoms remained constant, but different oxidation states occurred in the model. For instance, the model "disordered 2+" was obtained starting from the model "crystalline 2+" by moving nine oxygen atoms. Several models could be generated in this way. These models were screened in two ways. On the one hand, we used the total energy difference and the calculated bond energy penalties to derive an estimate for the amount of strain energy contained in the modified model. On the other hand, models with unphysical bond parameters could be excluded through the inspection of the bond angle and bond length distributions. In the retained disordered 2+ model, we tolerated an average strain energy of 0.18 eV per dislocated atom. Due to the increased disorder and the interrupted Si-Si chains in the final model, the band gap increased from 0.2 to 1.5 eV. For the model disordered 3+, two O atoms were moved, resulting in a strain energy contribution of 0.37 eV per displaced atom. In this case, the band gap decreased from 4.5 to 4.1 eV. During the relaxation process, the cell dimensions and the internal coordinates were allowed to vary, resulting in negligible changes of the density (see Table I).

IV. NITROGEN DANGLING BOND DEFECTS

A. Incorporation of N dangling bonds

Nitrogen dangling bond defects were generated by replacing one of the O atoms by nitrogen, except for the models of the second group which contained N dangling bond defects by construction. In the disordered models, the nitrogen substitution was carried out at different locations in order to sample a wide range of configurations. For every configuration considered, a full structural relaxation of the atomic coordinates was performed.

In the neutral state, the Si-N bond length averaged over the full set of available models was found to be 1.68 Å and its distribution showed a standard deviation of 0.04 Å. This value for the average bond length of twofold coordinated N atoms is only slightly smaller than that (1.76 Å) of threefold coordinated N atoms in the models of the second group. The Si-N-Si angular distribution shows an average value of 144° with a standard deviation of 12° and mainly reflects the spread of Si-O-Si angles of the parent structures.

For all models, we also considered charged states in which the extra charge is carried by localized states. In almost all models, the charge state −1 gave rise to such a localized state. This charge state corresponds to a doubly occupied dangling bond. The structure of the dangling bond defect underwent only minor changes: the average Si-N-Si angle did not change within 2° and the average Si-N bond length decreased by less than 0.1 Å.

In the SiO_2 models, localized states were also found for positive charge $q=+1$ and triplet spin state. Here, the average Si-N bond length elongated by less than 0.1 Å with respect to the neutral configuration, while the average Si-N-Si angle did not change significantly. To understand this unexpected spin state, the Kohn-Sham orbitals were inspected revealing an interaction between the N dangling bond and nearby O $2p$ orbitals belonging to the valence band. This stabilizing interaction is observed for a range of N-O distances which correspond to the range of typical O-O distances in a-SiO_2. However, since this interaction involves band-edge states, this result might be affected by the band-gap problem of the PBE scheme. As far as the present study is concerned, this charge state is not relevant for electron chemical potentials varying within the silicon band gap (see Sec. IV B 1).

To analyze the energetics associated to the N dangling bond defect, we define the formation energy E_f^q as a function of the electron chemical potential:[20]

$$E_f^q(\mu) = E_{tot}^q - E_{tot}^{ref} + q(\varepsilon_v + \mu + \Delta V) + E_{corr}, \quad (1)$$

where E_{tot}^q is the total energy of the defect in its charge state q and the electron chemical potential μ is referenced with respect to the top of the valence band ε_v of the defect-free oxide. The reference energy is set to

$$E_{tot}^{ref} = E(\text{oxide}) + E(N_2)/2 - E(O_2)/2, \quad (2)$$

where E(oxide), $E(N_2)$, and $E(O_2)$ are the total energies of the defect-free oxide and of the isolated N_2 and O_2 molecules, respectively. In this way, the formation energy $E_f^q(\mu)$ effectively describes the energy associated to the reaction

$$[\text{oxide}] + \frac{1}{2}N_2 \rightarrow [\text{oxide with } O \leftrightarrow N] + \frac{1}{2}O_2, \quad (3)$$

where "$O \leftrightarrow N$" represents the substitution of one O by one N. ΔV in Eq. (1) is a correction term that describes the potential shift when going from the system with defect to the defect-free model and amounts to at most 0.1 eV for our models. E_{corr} is a correction term that accounts for the spurious electrostatic interactions introduced by the periodic boundary conditions.[30] This correction terms depends on the static dielectric constant of the host oxide. We used $\epsilon=4$ for SiO_2. We obtained the dielectic constants for the substoichiometric oxides by linear interpolation, taking $\epsilon=12$ for Si. These assumptions are consistent with recent theoretical studies.[47,48] In Table I, we explicitly give the value of E_{corr} used for each model.

For the defect models that were not generated by $O \leftrightarrow N$ substitution, substitution energies were not calculated. To compare the total energies of different charge states in this case, we set $E_{tot}^{ref}=E_{tot}^0$ and referenced the electron chemical

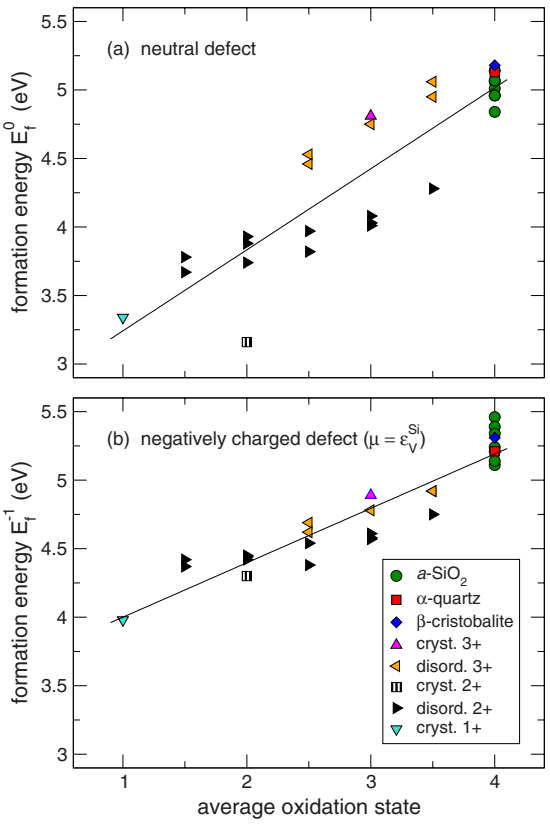

FIG. 6. (Color online) Formation energy (E_f^q) of the nitrogen dangling bond defect in (a) the neutral and (b) the negatively charged state as a function of the average oxidation state of the two nearest-neighbor silicon atoms. All models of the first and third group have been considered. The straight lines correspond to linear regressions.

potential with respect to the band edges of the amorphous SiO_2 model. This required the alignment of the electronic structures of the two models through the O 2*s* levels.

For the neutral N dangling bond defect, the substitution energy given by $E_f^0(\mu)$ does not depend on μ. In Fig. 6(a), this substitution energy is plotted as a function of the average oxidation state of the two nearest neighbor Si atoms for the defects in this work. The calculated substitution energy is found to be always positive, i.e., reaction (3) is endothermic. While the data are scattered because of the structural variety, one clearly recognizes a trend by which the nitrogen incorporation is favored in oxide environments showing lower oxygen content. This result is consistent with experimental observations which indicate that nitrogen incorporated at the Si/SiO_2 interface accumulates in the vicinity of the silicon substrate.[49,50] These results also emphasize the importance of investigating the nitrogen defect levels for varying oxygen concentration.

The formation energies of the defects in the negative charge state $q=-1$ depend on the electron chemical potential μ. To compare formation energies of different defects in this charge state, it is necessary to adopt a common value for μ. This is achieved by fixing the electron chemical potential in correspondence of the silicon valence band maximum, i.e., $\mu=\varepsilon_v^{Si}$. We emphasize that this alignment explicitly relies on the procedure described in Sec. II, involving the alignment of the O 2*s* levels and the use of the Si/SiO_2 band diagram. Figure 6(b) displays the formation energy E_f^{-1} ($\mu=\varepsilon_v^{Si}$) vs the average oxidation state of the two nearest-neighbor Si atoms for each considered defect. As for the neutral charge state, the formation energy is found to increase with oxidation state. The smaller slope compared to the neutral defect indicates that the negatively charged defects become relatively more stable as the dielectric constant drops, contrarily to expectations solely based on simple electrostatics arguments. This analysis does not change qualitatively when the dependence of the O 2*s* state on the oxidation states of the neighboring Si atoms [Fig. 2(b)] is considered in the alignment. This effect leads to an increase in the formation energies E_f^{-1} ($\mu=\varepsilon_v^{Si}$) by about 0.3 eV for the lowest oxidation states, thereby further reducing the slope in Fig. 6(b).

B. Charge transition levels of N dangling bonds

A charge transition level of a defect is defined as the value of the electron chemical potential for which two different charge states have the same formation energy E_f^q.

1. Stoichiometric SiO_2

For models of α quartz and amorphous SiO_2, we focused on three different charge states: $q=+1$, 0, and -1. Other charge states do not lead to charge transition levels in the oxide band gap. For each charge state, a full structural relaxation was carried out. Figure 7(a) shows the positions of the charge transition levels in the respective PBE band gaps. For α quartz, we found transition energies at $\varepsilon^{+/0}=0.2$ eV and $\varepsilon^{0/-}=2.4$ with respect to the PBE valence-band edge. The $0/-$ charge transition level is in accord with the result of a previous PBE calculation, which situated this level at 2.57 eV.[21,35] For the amorphous SiO_2 model, we considered seven different atomic configurations and obtained charge transition levels at $\varepsilon^{+/0}=0.1\pm0.4$ eV and $\varepsilon^{0/-}=2.2\pm0.1$ eV from the PBE valence band. The charge transition levels obtained for the disordered structure agree well with those of α quartz, as can be seen in Fig. 7(a), where the respective band structures have been aligned through the O 2*s* states. For our set of considered configurations, we did not detect any correlation between the energy of the transition levels and local structural parameters such as the Si-N bond length or the Si-N-Si angle.

Adopting the alignment scheme described in Sec. II, the calculated charge transition levels could be placed within the band diagram of the Si/SiO_2 interface [Fig. 7(b)]. In the case of α quartz, the charge transition levels occur at -2.1 and 0.1 eV with respect to the valence-band maximum of silicon [Fig. 7(b)]. For the amorphous SiO_2 model, these energies are -1.9 and 0.3 eV.

In the PBE, the $\varepsilon^{+/0}$ levels for both SiO_2 models fall only slightly above the valence-band edges. Hence, these levels might be affected by the PBE band-gap problem and their estimated energy in the Si/SiO_2 band diagram should be taken as an upper bound. Thus, our study reveals that the only defect level occurring within the silicon band gap is the

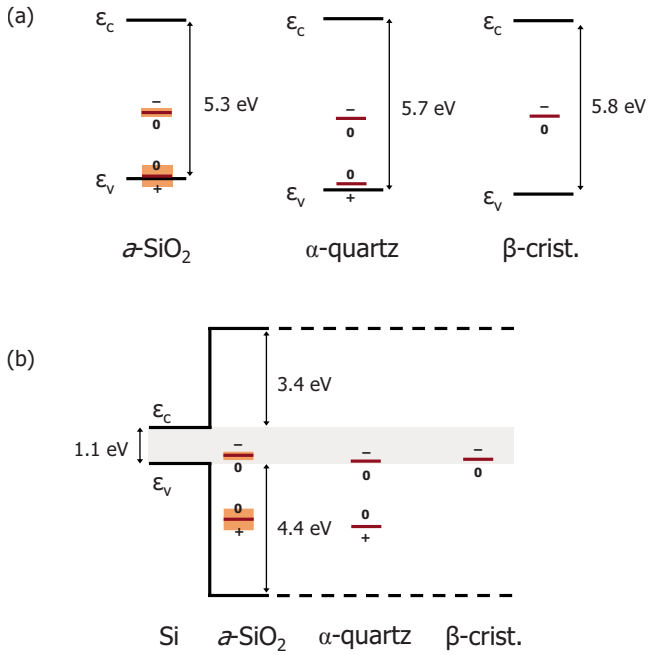

FIG. 7. (Color online) Charge transition levels of the N dangling bond in the stoichiometric SiO_2 models (a-SiO_2, α quartz, and β cristobalite) as found (a) with respect to the PBE band edges of their parent defect-free structures, aligned through their average O $2s$ level, and (b) within the Si/SiO_2 band diagram derived through the use of hybrid functionals. The pink/gray area in the case of a-SiO_2 represents the standard deviation resulting from seven different atomic configurations.

$0/-$ transition. In the following, we will only focus on this specific level.

In β cristobalite, the $0/-$ transition level is found at 2.6 eV above the PBE valence band edge. In the Si/SiO_2 band diagram, this level lies at 0.1 eV from the Si valence band.

2. Nitrided SiO_2

The classical models of nitrided SiO_2 incorporate the N atoms from the outset and therefore a defect-free host is unavailable for the determination of the valence-band edge. To overcome this problem, we determined the charge transition level with respect to the valence-band edge of a-SiO_2. The alignment between the two electronic systems was achieved through the levels of the deep O $2s$ states. The result of this alignment is shown in Fig. 8(a), where the $0/-$ charge transition level is found at 2.1 ± 0.2 eV from the PBE valence-band edge of a-SiO_2. When the band edges are shifted according to the results obtained with hybrid functional calculations (cf. Sec. II), the average transition level occurs at 0.1 eV from the Si valence-band edge [Fig. 8(b)]. This level should be compared with the average transition level calculated for N defects obtained by substitution in stoichiometric SiO_2 (Sec. IV B 1), which falls at 0.3 eV from the Si valence band. These results are consistent in view of the considered statistics, which give respective standard deviations of 0.2 and 0.14 eV. Hence, the different defect generation schemes used in the two cases do not appear to lead to any significant systematic difference.

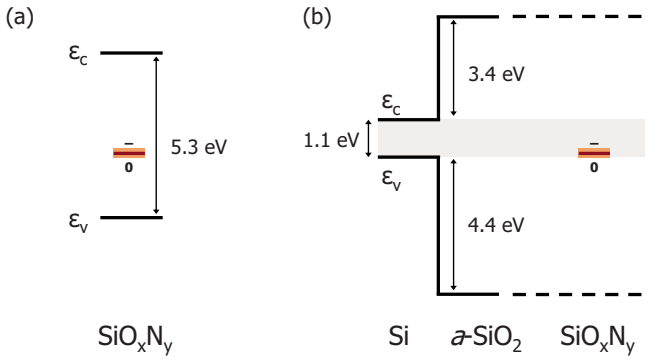

FIG. 8. (Color online) Charge transition levels of the N dangling bond in nitrided SiO_2 models (SiO_xN_y) as found (a) with respect to the PBE band edges of a-SiO_2 and (b) within the Si/SiO_2 band diagram derived through the use of hybrid functionals. The pink/gray area represents the standard deviation resulting from three different atomic configurations.

3. Substoichiometric oxides

The substoichiometric models with oxidation states 1+ and 2+ have a small band gap (cf. Table I) irrespective of structural disorder. For the crystalline 2+ model the negatively charged state of the N dangling bond gave rise to a delocalized state, suggesting that the $0/-$ transition level occurs below the valence band edge in our PBE calculations. For the crystalline 1+ and disordered 2+ models, we obtained localized states upon charging and the transition level occurred within the band gap. For the crystalline 3+ and disordered 3+ models, the band gap opens and their $0/-$ transition levels fall at 0.8 eV and 0.8 ± 0.1 eV from their respective valence-band edges. Figure 9(a) shows the calculated transition levels and the respective band edges for all the substoichiometric oxide models giving rise to localized defect states. Figure 9(b) shows these charge transition levels when reported within the band diagram of the Si/SiO_2 interface. The two models corresponding to the oxidation state 3+ show transition levels at 0.1 eV (crystalline 3+) and 0.0 ± 0.1 eV (disordered 3+) with respect to the Si valence band edge. The crystalline 1+ and disordered 2+ models gave slightly higher transition levels at 0.7 eV and 0.7 ± 0.1 eV from the silicon valence-band edge, respectively. The latter levels are expected to raise by an additional 0.3 eV upon consideration of the dependence of the O $2s$ level on the oxidation states of the neighboring Si atoms in the alignment [cf. Fig. 2(b)].

In Fig. 10, we display the $0/-$ charge transition levels as obtained for our full set of models vs the average oxidation state of the Si atoms neighboring the nitrogen dangling bond defect. The continuous line is obtained from the linear regressions in Figs. 6(a) and 6(b) describing the dependences of the formation energies on oxidation state for the neutral and the negatively charged state, respectively. The individual data points in Fig. 10 show significant scatter, which we attribute to structural disorder. However, a clear decreasing trend with increasing oxidation state is apparent and consistent with the continuous line derived from the formation energies. This dependence indicates that the charge transition

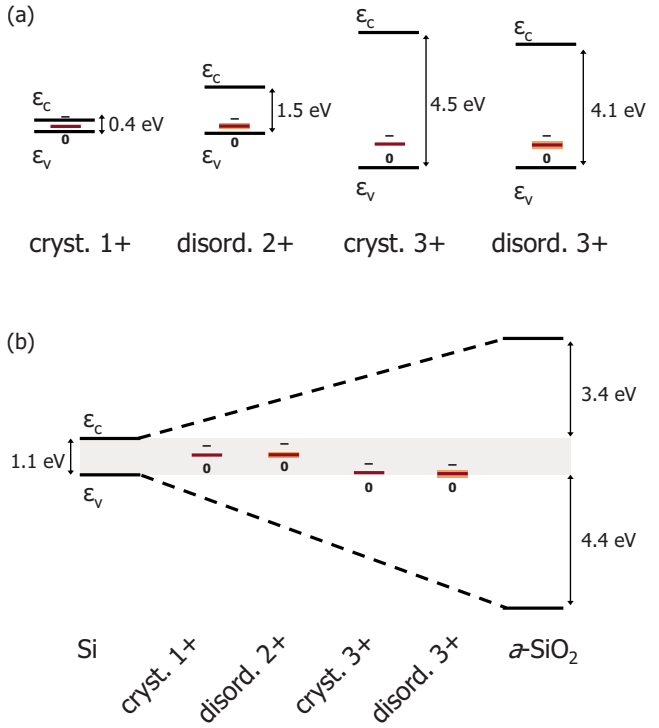

FIG. 9. (Color online) Charge transition levels of the N dangling bond in substoichiometric SiO_2 models (crystalline 1+, disordered 2+, crystalline 3+, and disordered 3+) as found (a) with respect to the PBE band edges of their parent defect-free structures aligned through their average O 2*s* level and (b) within the Si/SiO_2 band diagram derived through the use of hybrid functionals.

level rises across the silicon band gap when the defective nitrogen atom is found in a more silicon-rich environment, i.e., closer to the silicon substrate, where the nitrogen incorporation is energetically favored. The observed trend is further reinforced when the dependence of the O 2*s* level on oxidation state is considered in the alignment, leading to transition levels higher by 0.3 eV for the lowest oxidation states. In any case, all the charge transition levels fall below the silicon conduction band edge. Thus, our results indicate that the diamagnetic negatively charged dangling bond state is energetically favored for electron chemical potentials near the silicon conduction band, consistent with experimental EPR observations that the N dangling bond signal reduces upon electron injection.[18]

V. CONCLUSIONS

We determined the charge transition levels of nitrogen dangling bonds at the Si/SiO_2 interface within a density-functional scheme. To investigate the role of the composition grading in the interfacial region, we used various models of stoichiometric and substoichiometric silicon oxide and aligned their electronic structures through a separate interface calculation. Charge transition levels are calculated at the semilocal density functional level and then positioned with respect to the silicon band edges using a scheme based on hybrid functionals.[21,22] Only the 0/− charge transition level is found within the silicon band gap. In stoichiometric SiO_2,

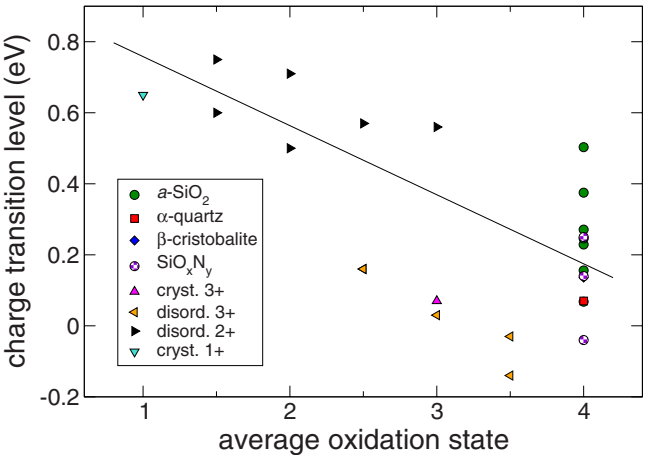

FIG. 10. (Color online) Charge transition levels 0/− of the nitrogen dangling bond in the oxide models considered in this work vs the average oxidation state of the two nearest-neighbor silicon atoms. The energies are referred to the silicon valence band edge, as determined through the use of hybrid functional calculations. The continuous line results from the linear regressions in Figs. 6(a) and 6(b).

this defect level is located in the lower part of the silicon band gap, but it is found to sweep across the gap as the nitrogen defects moves to more silicon-rich environments near the substrate, where the N incorporation is favored.

The present study might contribute to our understanding of the nitrogen-enhanced negative bias temperature instability, a reliability concern in MOS devices.[12,13] The reaction-diffusion model identifies depassivated Si dangling bonds as hole trapping centers for explaining the instability in *p*-channel MOS field-effect transistors.[13] Indeed, the interfacial Si dangling bond shows a 0/+ charge transition level at ~0.2 eV from the valence-band edge,[51,52] which allows for hole trapping. The present study shows that, in nitrided oxides, N dangling bonds also give interface states within the silicon band gap. The relevant transition corresponds to a negatively charged N dangling bond that turns into a neutral one upon hole trapping. In this way, the occurrence of depassivated nitrogen dangling bonds is expected to provide an extra channel for the negative bias temperature instability. However, in order to acquire a more comprehensive picture of the role of nitrogen at $Si-SiO_2$ interfaces, it will be necessary to go beyond the substitutional nitrogen studied in this work and to address the full variety of possible nitrogen configurations at the interface.

More generally, the present investigation illustrates a practical scheme for determining the energy levels of defects occurring in interfacial transition regions. In particular, it is worth highlighting two advantageous aspects of this scheme. First, the modeling of the transition region is achieved through a series of bulk models of different stoichiometry. With respect to the use of actual interface models, this approach not only allows for a broader statistical investigation, but also bypasses electrostatic complications due to the use of periodic simulation cells. The alignment of the electronic structures of the various bulk models is achieved through a model structure of the interface. Second, this work addresses

the issue of positioning defect levels calculated within a semilocal density-functional scheme with respect to an interfacial band diagram allowing for direct comparisons with experiments. This difficulty directly stems from the band-gap problem of semilocal density-functional schemes. Because of the underestimated band gaps and band offsets,[22] the position of the calculated defect levels is ambiguous.[21] To overcome this problem, we carried out all the defect-level calculations within a semilocal density-functional approach but relied on recent hybrid functional results to achieve a realistic description of the defect and band alignments. We used the fact that the position of defect levels with respect to a local reference potential as determined within a semilocal density-functional scheme remains unaffected by band-gap renormalization.[21] This result provides a justification for the *a posteriori* correction of the band edges. In our scheme, the band shifts are taken from a hybrid density-functional study which proved very successful in describing the experimental band alignment at the Si/SiO_2 interface.[22] In this way, the defect levels calculated in this study could be located with respect to the silicon band edges at the interface.

Despite these advantageous aspects, the presented scheme is nevertheless unable to capture structural and dielectric effects specific to the interface. These effects might become particularly severe in the close vicinity of the substrate, where dielectric relaxation effects become significant and where the crystallinity of the substrate might give rise to mechanical constraints. For the full consideration of these effects, the explicit modeling of the interface environment will be ineluctable.

ACKNOWLEDGMENTS

We thank A. Alkauskas and J. F. Binder for fruitful interactions. Support from the Swiss National Science Foundation (Grant No. 200020–119733/1) is acknowledged. The calculations were mainly performed on computational facilities at DIT-EPFL and CSEA-EPFL, but also at CSCS.

[1] S. Sze, *Physics of Semiconductor Devices* (John Wiley and Sons, New York, 1981).
[2] G. Kamarinos and P. Felix, J. Phys. D **29**, 487 (1996).
[3] J. H. Weil, J. R. Bolton, and J. E. Wertz, *Electron Paramegnetic Resonance: Elementary Theory and Practical Applications* (Wiley, New York, 1994).
[4] P. M. Lenahan and J. F. Conley, Jr., J. Vac. Sci. Technol. B **16**, 2134 (1998).
[5] K. L. Brower, Semicond. Sci. Technol. **4**, 970 (1989).
[6] D. Buchanan, IBM J. Res. Develop. **43**, 245 (1999).
[7] D. Mathiot, A. Straboni, E. Andre, and P. Debenest, J. Appl. Phys. **73**, 8215 (1993).
[8] C. H. Ang, S. S. Tan, C. M. Lek, W. Lin, Z. J. Zheng, T. Chen, and B. J. Cho, Electrochem. Solid-State Lett. **5**, G26 (2002).
[9] J. Ushio, T. Maruizumi, and K. Kushida-Abdelghafar, Appl. Phys. Lett. **81**, 1818 (2002).
[10] S. S. Tan, T. P. Chen, J. M. Soon, K. P. Loh, C. H. Ang, and L. Chan, Appl. Phys. Lett. **82**, 1881 (2003).
[11] S. Fujieda, Y. Miura, M. Saitoh, E. Hasegawa, S. Koyama, and K. Ando, Appl. Phys. Lett. **82**, 3677 (2003).
[12] D. K. Schroder and J. A. Babcock, J. Appl. Phys. **94**, 1 (2003).
[13] D. K. Schroder, Microelectron. Reliab. **47**, 841 (2007).
[14] Y. Cros and J. Krautwurm, J. Non-Cryst. Solids **187**, 385 (1995).
[15] L.-N. He, T. Inokuma, and S. Hasegawa, Jpn. J. Appl. Phys. **35**, 1503 (1996).
[16] S. Hasegawa, S. Sakamori, M. Futatsudera, T. Inokuma, and Y. Kurata, J. Appl. Phys. **89**, 2598 (2001).
[17] H. M. A. El-Oyoun, T. Inokuma, Y. Kurata, and S. Hasegawa, Jpn. J. Appl. Phys. **42**, 3570 (2003).
[18] I. A. Chaiyasena, P. M. Lenahan, and G. J. Dunn, Appl. Phys. Lett. **58**, 2141 (1991).
[19] C. K. Wong, H. Wong, V. Filip, and P. S. Chung, Jpn. J. Appl. Phys. **46**, 3202 (2007).
[20] C. G. Van de Walle and J. Neugebauer, J. Appl. Phys. **95**, 3851 (2004).
[21] A. Alkauskas, P. Broqvist, and A. Pasquarello, Phys. Rev. Lett. **101**, 046405 (2008).
[22] A. Alkauskas, P. Broqvist, F. Devynck, and A. Pasquarello, Phys. Rev. Lett. **101**, 106802 (2008).
[23] S. Ismail-Beigi and S. G. Louie, Phys. Rev. Lett. **95**, 156401 (2005).
[24] J. P. Perdew, K. Burke, and M. Ernzerhof, Phys. Rev. Lett. **77**, 3865 (1996).
[25] D. Vanderbilt, Phys. Rev. B **41**, 7892 (1990).
[26] A. Pasquarello, K. Laasonen, R. Car, C. Lee, and D. Vanderbilt, Phys. Rev. Lett. **69**, 1982 (1992).
[27] K. Laasonen, A. Pasquarello, R. Car, C. Lee, and D. Vanderbilt, Phys. Rev. B **47**, 10142 (1993).
[28] R. Fletcher, *Practical Methods of Optimization* (John Wiley and Sons, New York, 1987).
[29] P. Giannozzi, S. Baroni, N. Bonini, M. Calandra, R. Car, C. Cavazzoni, D. Ceresoli, G. L. Chiarotti, M. Cococcioni, I. Dabo, A. Dal Corso, S. de Gironcoli, S. Fabris, G. Fratesi, R. Gebauer, U. Gerstmann, C. Gougoussis, A. Kokalj, M. Lazzeri, L. Martin-Samos, N. Marzari, F. Mauri, R. Mazzarello, S. Paolini, A. Pasquarello, L. Paulatto, C. Sbraccia, S. Scandolo, G. Sclauzero, A. P. Seitsonen, A. Smogunov, P. Umari, and R. M. Wentzcovitch, J. Phys.: Condens. Matter **21**, 395502 (2009)
[30] G. Makov and M. C. Payne, Phys. Rev. B **51**, 4014 (1995).
[31] F. Giustino and A. Pasquarello, Phys. Rev. Lett. **95**, 187402 (2005).
[32] J. Godet, P. Broqvist, and A. Pasquarello, Appl. Phys. Lett. **91**, 262901 (2007).
[33] P. Broqvist, A. Alkauskas, and A. Pasquarello, Appl. Phys. Lett. **92**, 132911 (2008).
[34] P. Broqvist, A. Alkauskas, J. Godet, and A. Pasquarello, J. Appl. Phys. **105**, 061603 (2009).
[35] A. Alkauskas, P. Broqvist, and A. Pasquarello, in *AIP Proceedings of the 29th International Conference of the Physics of Semiconductors*, edited by M. J. Caldas and N. Studart (AIP, Melville, NY, 2009).
[36] R. Shaltaf, G.-M. Rignanese, X. Gonze, F. Giustino, and A. Pas-

quarello, Phys. Rev. Lett. **100**, 186401 (2008).
[37] A. Alkauskas, P. Broqvist, and A. Pasquarello, Phys. Rev. B **78**, 161305(R) (2008).
[38] S. Coh and D. Vanderbilt, Phys. Rev. B **78**, 054117 (2008).
[39] F. Liu, S. H. Garofalini, R. D. King-Smith, and D. Vanderbilt, Phys. Rev. Lett. **70**, 2750 (1993).
[40] J. Sarnthein, A. Pasquarello, and R. Car, Phys. Rev. B **52**, 12690 (1995).
[41] J. Sarnthein, A. Pasquarello, and R. Car, Phys. Rev. Lett. **74**, 4682 (1995).
[42] W. L. Scopel, A. J. R. da Silva, W. Orellana, R. J. Prado, M. C. A. Fantini, A. Fazzio, and I. Pereyra, Phys. Rev. B **68**, 155332 (2003).
[43] D. R. Hamann, Phys. Rev. B **61**, 9899 (2000).
[44] J. F. Binder, P. Broqvist, and A. Pasquarello, Microelectron. Eng. **86**, 1760 (2009).
[45] A. Bongiorno and A. Pasquarello, Phys. Rev. B **62**, R16326 (2000).
[46] F. Giustino, A. Bongiorno, and A. Pasquarello, J. Phys.: Condens. Matter **17**, S2065 (2005).
[47] F. Giustino and A. Pasquarello, Surf. Sci. **586**, 183 (2005).
[48] F. Giustino and A. Pasquarello, Phys. Rev. B **71**, 144104 (2005); F. Giustino, P. Umari, and A. Pasquarello, Phys. Rev. Lett. **91**, 267601 (2003).
[49] D. G. J. Sutherland *et al.*, J. Appl. Phys. **78**, 6761 (1995).
[50] S. R. Kaluri and D. W. Hess, Appl. Phys. Lett. **69**, 1053 (1996).
[51] E. H. Poindexter, G. J. Gerardi, M.-E. Rueckel, P. J. Caplan, N. M. Johnson, and D. K. Biegelsen, J. Appl. Phys. **56**, 2844 (1984).
[52] P. Broqvist, A. Alkauskas, and A. Pasquarello, Phys. Rev. B **78**, 075203 (2008).